Archives of Acoustics Vol. 48, No. 4, pp. 529–538 (2023), doi: 10.24425/aoa.2023.146813

Research Paper

A Multi-Layer Micro-Perforated Panel Structure Based on Curled Space for Broadband Sound Absorption at Low Frequencies

Jiaming CHU[(1)], Xiao LIANG[(1),(2)*], Zhen YANG[(1)], Haofeng LIANG[(1)], Tao CHEN[(1)], Liang SU[(1)], Zhuo ZHOU[(3)*]

[(1)] *School of Mechanical Engineering, Xiangtan University*
Xiangtan, China

[(2)] *Foshan Green Intelligent Manufacturing Research Institute of Xiangtan University*
Foshan, Guangdong, China

[(3)] *School of Mechanical Engineering and State Key Laboratory for Strength and Vibration of Mechanical Structures Xi'an Jiaotong University*
Xi'an, Shanxi, China

*Corresponding Authors e-mails: liangxiao@xtu.edu.cn (Xiao Liang); zhouzhuo221@163.com (Zhuo Zhou)

(*received February 16, 2023; accepted May 19, 2023*)

In this paper, we propose a multi-layer micro-perforated panel structure based on a curled space for broadband sound absorption at low frequencies, which increases the number of perforated panel layers in a limited space using a curled space. The absorption coefficients of the structure under plane wave conditions were calculated using the transfer matrix method and the finite element method. It is demonstrated that the multi-layer micro-perforated panel structure can ensure high absorption (consistently over 90%) in the frequency range of 400~5000 Hz. The sound absorption mechanism of the multi-layer micro-perforated panel structure is investigated by using the acoustic impedance along with the reflection coefficient of the complex frequency surface. In addition, we also discuss the effects of the micro-perforated panel parameters on the structural sound absorption coefficient. The results show that the proposed multi-layer micro-perforated panel structure provides an excellent solution for sound absorption in a limited space.

Keywords: micro-perforated plate; curled space; broadband sound absorption; complex frequency plane method.

1. Introduction

The micro-perforated plate (MPP) has an excellent broadband sound absorption ability, as well as high-temperature resistance, corrosion resistance, and non-pollution, which is regarded as one of the most promising next-generation sound absorption materials. Maa (1983) first proposed the concept of the MPP absorber by reducing the diameter of perforations in conventional perforated plates to less than one millimeter, thus obtaining the MPP structure with high acoustic resistance and low acoustic impedance. Since then, MPP absorbers have received widespread attention in various acoustic applications.

Currently, the theory of MPP has been widely studied (Cheng, 2018; Rafique *et al.*, 2021; Li, 2018). Maa (1984, 1994) provided the MPP theoretical analysis and design principles. In addition, the double-layer MPP structure was developed to expand further the sound absorption band (Maa, Liu, 2000). As compared to the narrower absorption band of the single-layer MPP structure, the double-layer MPP produces two different absorption peaks, thus obtaining a wider absorption band. Mosa *et al.* (2020b) introduced inhomogeneous perforations on top of the double-layered MPP, which further increased the absorption band. At the same time as introducing inhomogeneous perforations, Mosa *et al.* (2020a) set up multiple cavities

with different depths to produce a wider absorption band. Due to the mutual coupling of multiple absorption peaks, the MPP can form a wide band of sound absorption, therefore, there are several studies based on a multi-layer MPP. For example, Cobo *et al.* (2019) designed a three-layer MPP and optimized the MPP parameters by a simulated annealing method. Bucciarelli *et al.* (2019) established an analytical model for the design of multi-layer MPP absorbers and found that adding more MPP leads to resonant coupling, which is beneficial to improve the absorption band. In addition, it obtained the 5-layer MPP structure. By optimizing the parameters of the MPP structure, the absorption coefficient of this structure at 400~2000 Hz is all over 0.9. Using the transmission matrix method is more convenient than the equivalent circuit analysis method to study a multi-layer MPP (Lee, Kwon, 2004). Carbajo *et al.* (2020) proposed the multi-layer MPP absorber with inclined perforations and investigated its acoustic properties using the transfer matrix method, which promotes the application of a multi-layer MPP in the field of noise reduction.

A multi-layer MPP has broad-frequency sound absorption characteristics, however, a large cavity is often required for low-frequency sound absorption, which significantly limits its application (Zhao, Lin, 2022). Many studies have proposed solutions to this problem. Firstly, in response to the crisis of excessive cavity volume, Li and Assouar (2016) significantly reduced the structural volume by converting the cavity into a coiled coplanar air chamber, which absorbed sound perfectly at 125 Hz. Similarly, Prasetiyo *et al.* (2021) introduced a coiled structure in the cavity to reduce the cavity volume, and the absorption coefficients exceeded 0.8 from 250 to 1000 Hz. Cui *et al.* (2022) also obtained a composite spatially folded metamaterial structure by a curled space and achieved a large broadband absorption above 200 Hz. It is a simple and practical way to reduce the cavity volume by spatially coiled structures, and there are many similar studies (Liu *et al.*, 2019; 2020; Wu *et al.*, 2019). Secondly, MPP structures are often used together with other structures to improve low-frequency sound absorption further to obtain new acoustic metamaterials (Cheng *et al.*, 2022; Gao *et al.*, 2017; Rafique *et al.*, 2022). Xiaoqi and Cheng (2021) achieved broadband and low-frequency sound absorption by setting MPP boundaries in an acoustic black hole structure. Shao *et al.* (2022) designed a tunable multi-layer composite structure by combining the Helmholtz structure, MPP, and porous material, which has absorption coefficients exceeding 0.9 at 400~3000 Hz. Xie *et al.* (2022) combined the MPP structure with a conchoidal cavity structure. The structural absorption band can be changed by adjusting the structural parameters.

A multi-layer MPP has broad frequency sound absorption characteristics and the coiled structure can reduce the volume of the structure. Based on these two characteristics, this paper investigates the acoustic performance of the multi-layer MPP with a coiled structure. Moreover, we study the sound absorption mechanism using the complex frequency surface acoustic impedance and the reflection coefficient. In addition, we discuss the effect of perforated panel parameters on the sound absorption coefficient of the structure. Finally, it is shown that sound absorption can be achieved at different frequency bands by changing the perforated panel parameters and structure dimensions.

2. Theoretical analysis

2.1. Basic formulations

According to Maa's approximation formula (Maa, 1998), the single-layer MPP relative acoustic impedance can be written as:

$$z_{\mathrm{MPP}} = r + j\omega m, \tag{1}$$

where j is the imaginary number, ω is the angular frequency, r is the relative acoustic resistance, and m is the relative acoustic mass, which are defined as:

$$r = \frac{32\eta t}{\rho c \sigma d^2}\left[\left(1+\frac{x^2}{32}\right)^{\frac{1}{2}} + \frac{\sqrt{2}}{8}\frac{xd}{t}\right], \tag{2}$$

$$m = \frac{t}{\sigma c}\left[1+\left(9+\frac{x^2}{2}\right)^{-\frac{1}{2}} + 0.85\frac{d}{t}\right], \tag{3}$$

where $\eta = 1.8\times10^{-5}$ Pa·s, $\rho = 1.25$ kg/m^3, $c = 343$ m/s are the dynamic viscosity coefficient, the density, and sound speed of the air, t is the panel thickness, σ is the perforation ratio, and d is the diameter of the perforation hole, x is the perforation constant, and it is given by:

$$x = \frac{d}{2}\sqrt{\frac{\omega\rho}{\eta}}. \tag{4}$$

At the vertical incidence of plane waves, the sound absorption coefficient of a single-layer MPP can be expressed as:

$$\alpha = \frac{4r}{(1+r)^2 + \left(\omega m - \cot\left(\omega D/c\right)\right)^2}, \tag{5}$$

where D is the depth of the dorsal cavity of the MPP.

Further, we can simplify it to the following equation:

$$\alpha = \frac{4r}{(1+r)^2 + m'^2}. \tag{6}$$

By analyzing Eq. (6), we can discover that perfect sound absorption can only be achieved if $r = 1$ and $m' = 0$. In general, achieving an ideal acoustic impedance match for a wide frequency absorption

is not easy. However, in most practical applications, achieving perfect sound absorption is unnecessary, and absorbing most of the sound energy can also achieve the purpose. Therefore, this gives a larger range of acoustic impedance matches. As shown in Fig. 1, the sound absorption coefficients are shown for different relative sound impedances and sound masses. When the relative acoustic impedance is within the blue elliptical region in Fig. 1b, the sound absorption coefficient is above 0.8. At this time, the relative acoustic impedance region is significantly larger, dramatically reducing the structure requirements. For example, the MPP achieves the maximum absorption coefficient of 0.99 at 125 Hz when d, t, D, and σ are taken as 3.5, 0.2, 734 mm, and 0.096%, respectively. At this time, r and m' are 0.99 and −0.06, respectively, which are very close to the parameters at the theoretical maximum absorption coefficient. However, the sound absorption frequency band of a MPP is very narrow under this parameter. Moreover, the depth of the back cavity is too large. When D changed to 200 mm, the absorption coefficient of a MPP would reach 0.88 at 551 Hz (r = 2.06, m' = 0.05), and almost no absorption effect at 125 Hz (r = 0.99, m' = 148.5).

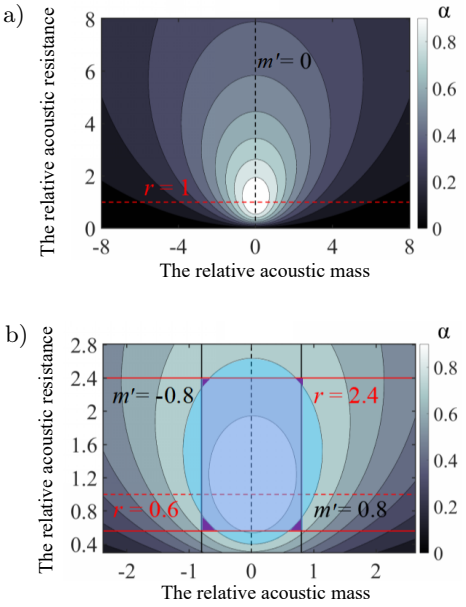

Fig. 1. MPP absorption coefficients at different relative acoustic impedances: a) the red and black dashed lines and intersection points represent r = 1, m' = 0, and α = 1, respectively; b) most of the region with $\alpha \geq 0.8$ is in the region bounded by $2.4 \geq r \geq 0.6$ and $-0.8 \geq r \geq 0.8$ (except for the purple region), which we refer to as region A.

2.2. Transfer matrix method

The transfer matrix method (TMM) is a simple method for the study of a multi-layer MPP. According to (Lee, Kwon, 2004), we can initially write the MPP and cavity transfer matrix, respectively:

$$[\mathbf{P}] = \begin{bmatrix} 1 & \rho c z_{\mathrm{MPP}} \\ 0 & 1 \end{bmatrix}, \tag{7}$$

$$[\mathbf{S}] = \begin{bmatrix} \cos(kh) & (j\rho c)\sin(kh) \\ (j/\rho c)\sin(kh) & \cos(kh) \end{bmatrix}, \tag{8}$$

where $k = \omega/c$ is the wave number, and h is the air cavity depth.

For a multi-layer MPP shown in Fig. 2, we can multiply the transfer matrix $\mathbf{P}_i$ of each MPP with the transfer matrix $\mathbf{S}_i$ of the air cavity sequentially, thus obtaining the total transfer matrix:

$$[\mathbf{T}] = [\mathbf{P}]_1 [\mathbf{S}]_1 \cdots [\mathbf{P}]_n [\mathbf{S}]_n = \begin{bmatrix} T_{11} & T_{12} \\ T_{21} & T_{22} \end{bmatrix}. \tag{9}$$

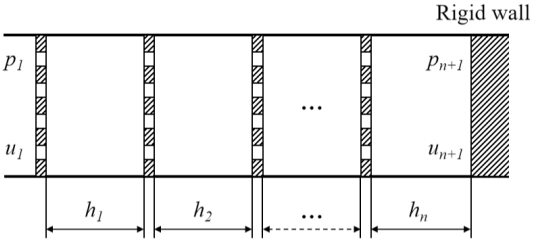

Fig. 2. Schematic diagram of the multi-layer MPP structure.

At the vertical incidence of plane waves, the reflection and absorption coefficients of a multi-layer MPP can be expressed as:

$$\gamma = \frac{T_{11} - \rho c T_{21}}{T_{11} + \rho c T_{21}}, \tag{10}$$

$$\alpha = \frac{4\,\mathrm{Re}\left(\frac{T_{11}/T_{21}}{\rho c}\right)}{\left[1 + \mathrm{Re}\left(\frac{T_{11}/T_{21}}{\rho c}\right)\right]^2 + \left[\mathrm{Im}\left(\frac{T_{11}/T_{21}}{\rho c}\right)\right]^2}. \tag{11}$$

The equivalent relative acoustic impedance and equivalent relative sound mass of a multi-layer MPP can also be calculated as:

$$z_0 = \frac{T_{11}/T_{21}}{\rho c}, \tag{12}$$

$$r_0 = \mathrm{Re}\left(\frac{T_{11}/T_{21}}{\rho c}\right), \tag{13}$$

$$m_0 = \mathrm{Re}\left(\frac{T_{11}/T_{21}}{\rho c}\right). \tag{14}$$

2.3. Finite element method

The 3D model of the structure is shown in Fig. 3a, where L = 121 mm and W = 48 mm are the length and width of the structure, respectively. As a result

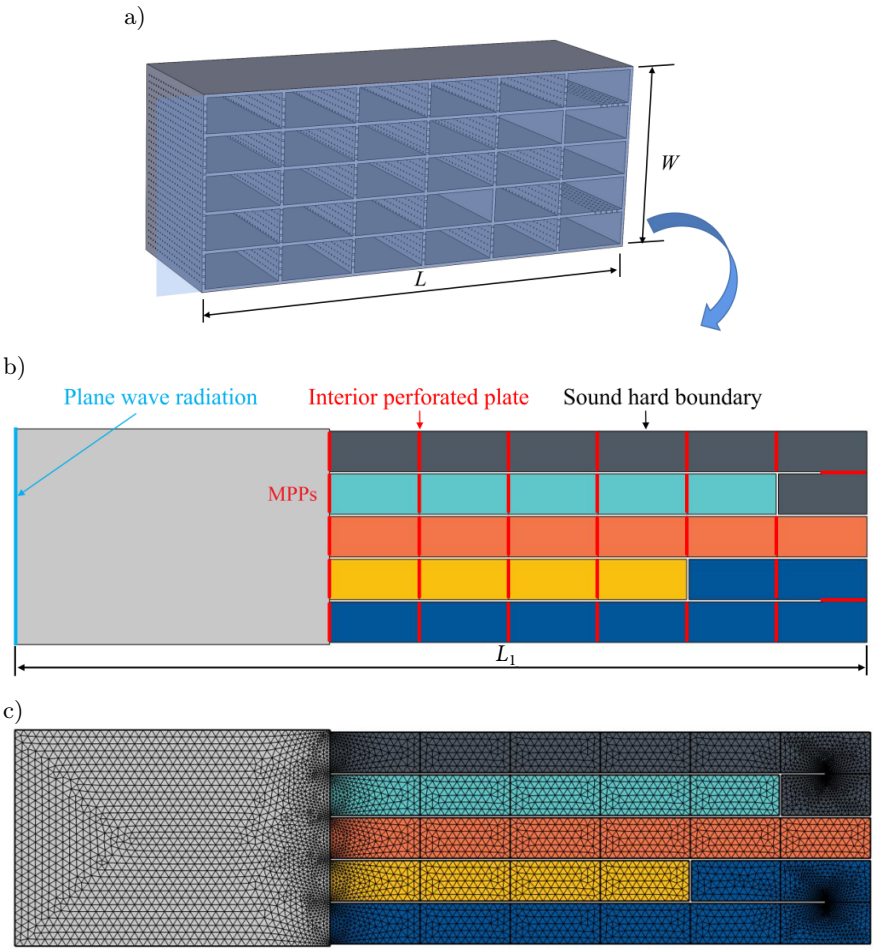

Fig. 3. Diagram of multi-layer MPP structure based on curl space: a) schematic diagram of the 3D model of the structure; b) finite element boundary conditions; c) finite element meshing.

of the symmetry of the 3D model, we reduce the 3D model to a 2D planar model when performing the finite element simulation, as shown in Fig. 3b. The physical field under study is the Pressure Acoustic Frequency Domain and the entire study domain is the air domain, moreover the entire air domain length L_1 = 190 mm. The aero-domain and internal MPPs are modeled with a linear elastic fluid model and a thin-plate MPP model from COMSOL, respectively. In addition, the mesh is divided into free triangular meshes, and the maximum mesh is $^1/_{12}$ of the minimum wavelength to ensure the accuracy of the calculation. The sound incident field is a plane wave incident vertically, as shown by the blue line in Fig. 3b, and it is:

$$p_b = p_0 e^{-jkx}, \tag{15}$$

where p_0 = 1 Pa is the pressure amplitude.

The red line represents the interior perforated plate, whose diameter, thickness, and perforation rate are d = 0.2 mm, t = 0.1 mm, and σ = 0.03, respectively, and whose relative acoustic impedance can be expressed as:

$$z = \frac{j\omega\left(t + 8\,\mathrm{d}\, f_{\mathrm{int}}/3\pi\right)/c\sigma C_D}{J_2\left(d\sqrt{-ik}/2\right)/J_0\left(d\sqrt{-ik}/2\right)}, \tag{16}$$

where C_D = 1 and f_{int} represent the flow coefficient and the hole-hole interaction function, respectively; J_2 and J_0 are Bessel functions of the first kind of the second and first order.

The other boundaries of the model are the sound hard boundary, which means that the normal derivative of the pressure is zero at the boundary and they are:

$$\frac{\partial p_t}{\partial \mathbf{n}} = 0. \tag{17}$$

2.4. Sound absorption coefficient

According to (Zhao, Lin, 2022), the double-layer MPP can be flipped and thus reduce the back cavity space, as shown in Figs. 4a and 4b. Among them, the main parameters of the MPP structures include the plate thickness t_1 = 0.4 mm, hole diameter d_1 = 0.3 mm, the perforation rate σ_1 = 0.01, and the back cavity depth $D_1 = D_2$ = 75 mm. The research results show that the sound absorption coefficients of both are almost the same (Zhao, Lin, 2022). Therefore, we can approximate the equivalence of the two in our study, thus simplifying the calculation. The simplified model

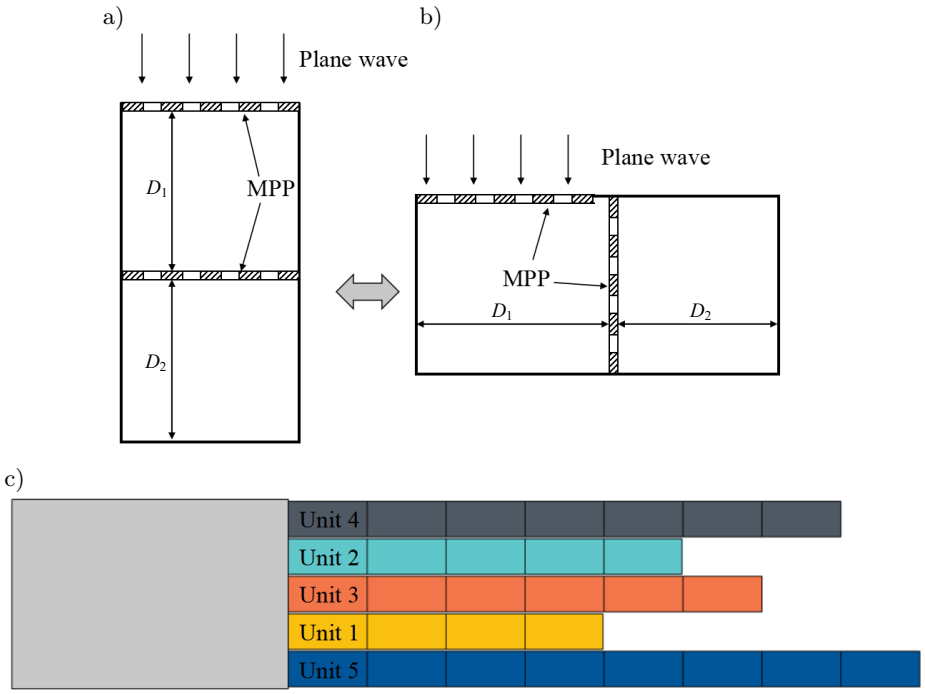

Fig. 4. Schematic diagram of two double-layer MPP structures and simplified model structure diagram: a) a conventional double-layer MPP; b) a turned double-layer MPP; c) a simplified model structure diagram.

structure is shown in Fig. 4c. The structure can be divided into 5 units, each of which is a multi-layered MPP structure and the number of layers increases from 4 to 8 layers sequentially. Furthermore, we number the units sequentially according to the number of layers of the MPP. Further, each unit can again be understood as a concrete example of the structure of Fig. 2.

Since the parameters of a MPP (d = 0.2 mm, t = 0.1 mm, σ = 0.03, and the spacing between adjacent MPPs is 20 mm) are consistent across the layers studied, Eq. (9) can be simplified and the transfer matrix of each unit can be expressed as:

$$[\mathbf{T}]_m = \{[\mathbf{P}][\mathbf{S}]\}^n \begin{cases} m = 1, 2, ..., 5, \\ n = 4, 5, ..., 8. \end{cases} \tag{18}$$

The equivalent relative acoustic impedance of each unit can be obtained by Eq. (12), and then the relative acoustic impedance of the structure as a whole can be obtained by the following equation:

$$\frac{S}{z_{eq}} = \frac{1}{\sum_{m=1}^{5} \frac{S_m}{z_m}}, \tag{19}$$

where S and S_m represent the acoustic incident area and the unit acoustic incident area, respectively, and $S = 5S_m$.

Eventually, at the vertical incidence of plane waves, the sound absorption coefficient of the structure can be expressed as:

$$\alpha = \frac{4\,\mathrm{Re}\,(z_{eq})}{[1 + \mathrm{Re}\,(z_{eq})]^2 + [\mathrm{Im}\,(z_{eq})]^2}. \tag{20}$$

The sound absorption coefficients calculated by FEM and TMM are shown in Fig. 5a, and the results of both calculations match satisfactorily. The reason for the slight error is that the FEM modeling considers the structure thickness. However, the effect of this on the analytical study is not significant. The absorption coefficient of the structure at 400~5000 Hz consistently exceeds 0.9, which has a wide absorption band. The equivalent acoustic impedance of the structure

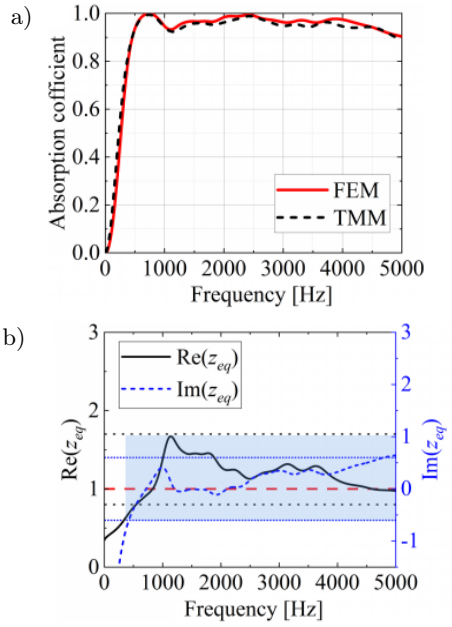

Fig. 5. Diagram of: a) the structural sound absorption coefficient; b) the relative acoustic impedance of the structure.

that will be derived according to Eq. (19) is shown in Fig. 5b. It can be seen from the figure that the relative acoustic impedance is not perfectly matched, but most of them are in region A (the region shown in Fig. 1b). Therefore, the absorption coefficient is more extensive than 0.8 in these frequency bands, which is an excellent verification of the sound absorption effect of the structure.

3. Parametric study

To better understand the effects of different design parameters on the sound absorption performance of the structure, a series of parametric studies are conducted in this section by varying parameters such as perforated plate thickness, perforation hole diameter, and perforation rate by using FEM simulations. In addition, the number of perforated plate layers, the unit distribution, and the size of the structure are also analyzed.

3.1. Effects of the perforation hole diameter

In order to better find out the effect of a perforation hole diameter on the sound absorption performance of the multi-layer MPP structure based on a curl space, we only change the value of the hole diameter d and keep other parameters constant. The results are shown in Fig. 6a, and it can be seen that choosing the proper aperture size is necessary to get the effect of broadband-efficient sound absorption. As the aperture diameter gradually increases, the peak absorption coefficient moves toward lower frequencies and more absorption lows appear. In the latter case, it is caused by an acoustic impedance mismatch. For the former, we analyzed the single small hole of the MPP and the air back cavity, which would be the Helmholtz resonator. Furthermore, it can be reduced to a spring oscillator and its resonant frequency is proportional to $\sqrt{K/M}$. As the hole diameter increases, the stiffness factor of the equivalent air spring K decreases. These are because at the constant perforation rate σ, an increase in the hole diameter causes a decrease in the number of holes and thus an increase in the volume of the air back cavity corresponding to each small hole. There is also an increase in the oscillator mass M due to the increase in the aperture diameter. Therefore, the peak absorption coefficient will be shifted towards the lower frequencies.

3.2. Effects of the panel thickness

As shown in Fig. 6b, the effect of the thickness of the MPP on the absorption coefficient of the multi-layer MPP structure based on a curl space is shown. It can be seen from the figure that as the thickness of the MPP increases, the sound absorption coefficient decreases. According to Eq. (16), the acoustic impedance of the MPP increases when t rises, which leads to a decrease in the absorption coefficient. Moreover, this parameter has a significant influence on the sound absorption coefficient, thus, it must be chosen reasonably.

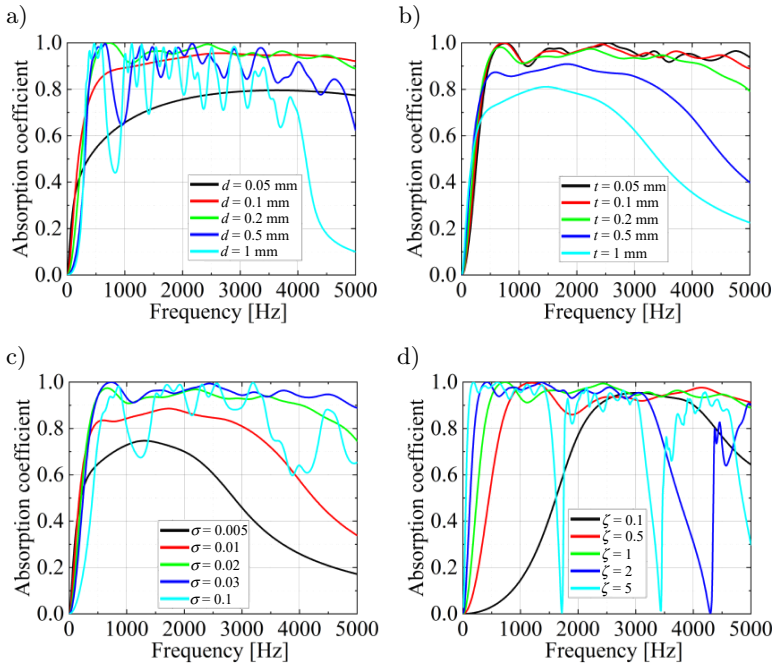

Fig. 6. Effect of different design parameters on the sound absorption coefficient of multi-layer MPP structure based on curl space: a) effects of the perforation hole diameter, t = 0.1 mm, σ = 0.03, h = 20 mm; b) effects of the panel thickness, d = 0.2 mm, σ = 0.03, h = 20 mm; c) effects of the perforation ratio, d = 0.2 mm, t = 0.1 mm, h = 20 mm; d) sound absorption coefficients of the structure with a different scale size, d = 0.2 mm, t = 0.1 mm, σ = 0.03, h = 20 mm.

3.3. Effects of the perforation ratio

In this subsection, we investigate the effect of the perforation rate σ on the structural absorption coefficient. The results are shown in Fig. 6c, the absorption coefficient increases, and the peak shifts to high frequencies when the perforation rate σ is increased. According to Eqs. (2), (3), and (16), we can know that the relative acoustic impedance of the MPP decreases as σ increases, which leads to an increase in the absorption coefficient. Similarly, by analogy with the spring oscillator model, we can find the reason for the peak shift to high frequencies. As σ increases, the equivalent air spring stiffness factor K increases, and M is constant, therefore the peak absorption coefficient moves to higher frequencies.

3.4. Effects of the structure with different scale sizes

In this subsection, the effect of the structure size on the absorption coefficient is studied, with ζ being the scaling ratio of the structure. The results are shown in Fig. 6d, the absorption coefficient peak will be moved to high frequencies when scaling down the structure as a whole. When scaled down to 0.5 times the structure, the sound absorption band will be in the middle and high frequencies (above 1000 Hz). When the structure is reduced to 0.1 times the structure, the absorption band will be at a high frequency (above 2400 Hz). On the contrary, the low-frequency sound absorption effect is enhanced by enlarging the structure. This is mainly caused by the change of cavity in the structure, the large cavity is more suitable for low-frequency sound absorption, but the larger structure size will also be detrimental to the actual use. Therefore, we can choose the corresponding structure size according to the real situation.

4. Sound absorption mechanism

4.1. Acoustic impedance analysis

In order to explain the principle of efficient sound absorption by MPP broadband, the relative acoustic impedance of the overall structure and each unit is analyzed in this subsection, and the calculation results are shown in Fig. 7. Also, all MPP parameters studied are the identical, $d = 0.2$ mm, $t = 0.1$ mm, $\sigma = 0.03$. In Fig. 7, the thick black solid line and the thick blue dashed line indicate the relative sound resistance and the relative sound mass, respectively. The critical values in Fig. 1b are shown as thin dashed lines in Fig. 7, where the blue shading is the frequency band when the absorption coefficient is more significant than 0.8. From Figs. 7a–7e, it can be seen that as the number of MPP layers increases, the peak of the relative acoustic impedance increases and moves toward the lower frequencies. In addition, the sound absorption band becomes gradually wider. This indicates that the multi-layer MPP structure favors low-frequency broadband sound absorption. For the multi-layer MPP structure based on a curl space,

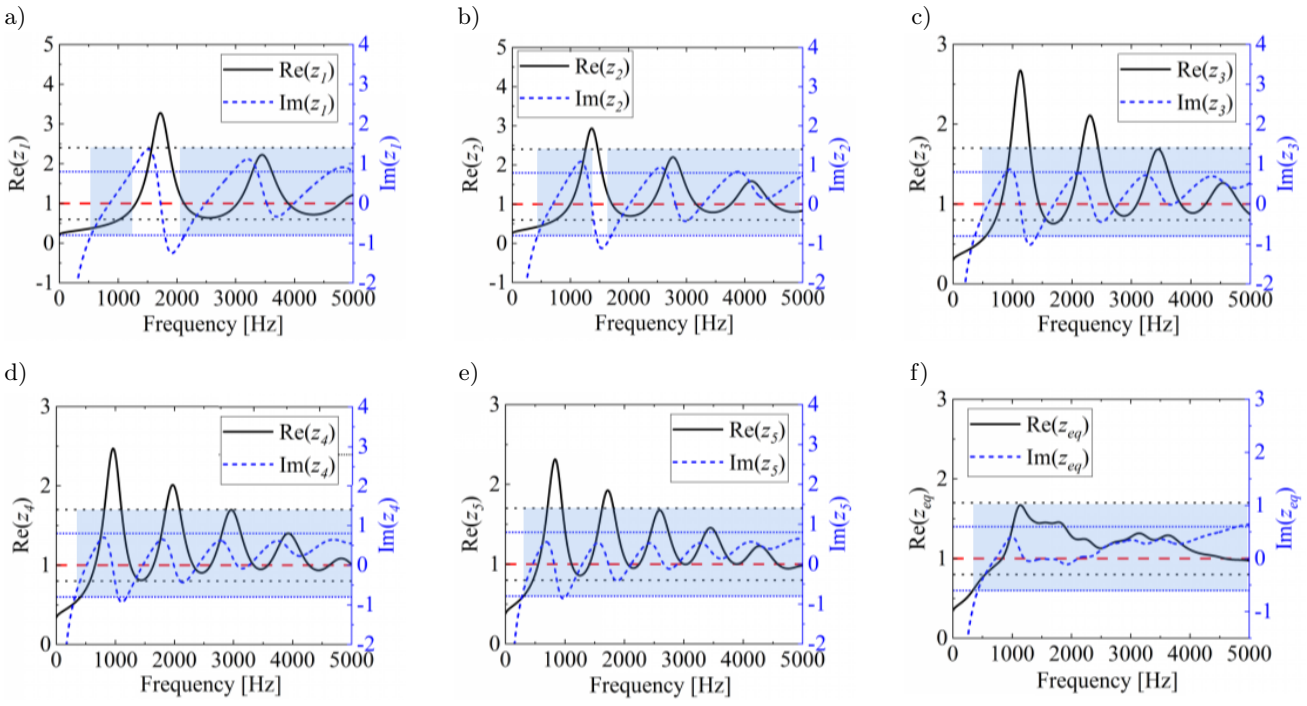

Fig. 7. Relative acoustic impedance of multi-layer MPP structures and their structural units based on curled space: a) unit 1 (4-layer MPP); b) unit 2 (5-layer MPP); c) unit 3 (6-layer MPP); d) unit 4 (7-layer MPP); e) unit 5 (8-layer MPP); f) the overall structure.

the parallel coupling of five units dramatically reduces the peak of the relative acoustic impedance, making the relative acoustic resistance and the relative sound mass closer to 1 and 0, respectively. Therefore, this also ensures the sound absorption effect at low frequencies and broadband sound absorption.

4.2. Complex frequency plane analysis

To further understand the absorption mechanism, we use a graphic approach to evaluate the reflection coefficient r in the complex plane (Jiménez *et al.*, 2017a; 2017b; Romero-García *et al.*, 2016). In general, in the lossless case, the reflection coefficient has a complex conjugate zero and a conjugate pole. When the loss balances the energy leakage, the zero falls exactly on the real frequency axis, meaning that the critical coupling condition is satisfied. In addition, the leakage rate between the zero point and the pole can determine the absorption bandwidth (Romero-García *et al.*, 2016). For example, as shown in Fig. 8c, there are three zeros and three poles, respectively. The zero point at 4000 Hz is very close to the real frequency axis, thus it will tend to perfect sound absorption.

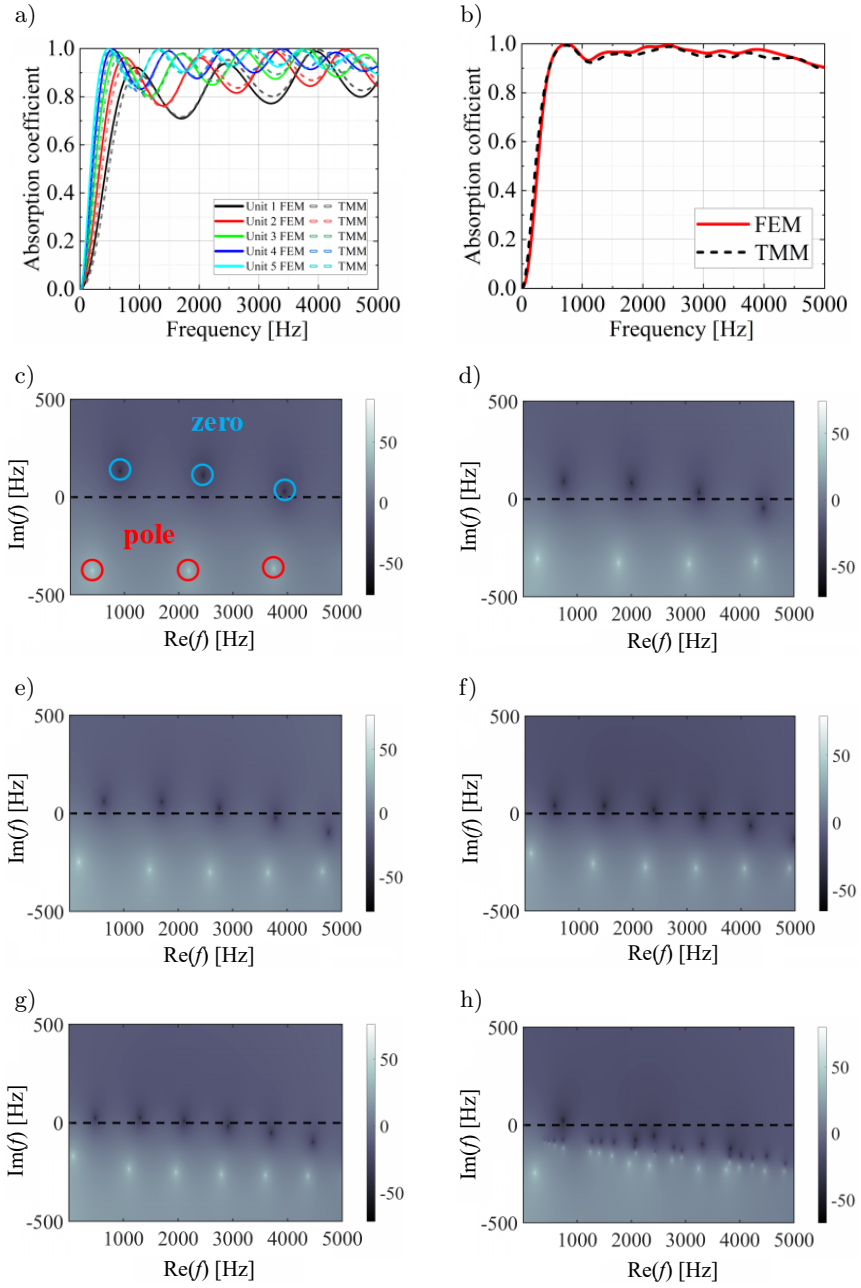

Fig. 8. a) and b) are the sound absorption coefficients of the five units and the overall structure, respectively; c)–h) are the representation of the $20\log_{10}|\gamma|$ in the complex frequency plane for the multi-layer MPP structures and their structural units based on curled space; c) unit 1 (4-layer MPP); d) unit 2 (5-layer MPP); e) unit 3 (6-layer MPP); f) unit 4 (7-layer MPP); g) unit 5 (8-layer MPP); h) the overall structure.

In addition, there is a large leakage rate between the zero and pole points that extends the absorption band. However, the absorption valley will be lower because of fewer resonance peaks. These can be seen from the absorption curves in Fig. 8a. As can be seen in Figs. 8c–8g, further increasing the number of layers of MPP can obtain more resonance peaks, yet it is not effective in reducing the leakage rate. Therefore, there are still many sound absorption valleys in multi-layer MPP structures.

The zero point is almost always below the real frequency axis for the multi-layer MPP with a coiled structure, as shown in Fig. 8h. Although the critical coupling condition is not fully satisfied, a high absorption is still obtained at the resonant frequency. In addition, the leakage rate between zero and the pole is small and the number of resonance peaks is large. With the combined effect of these two reasons, both lower absorption valleys are eliminated and broadband absorption is achieved. As shown in Fig. 8b, the absorption curve consistently exceeds 0.9 in the 400~5000 Hz frequency range, and half absorption is achieved at 230 Hz.

5. Conclusions

This paper proposes a multi-layer micro-perforated panel structure based on a curled space for broadband sound absorption at low frequencies. The structure is approximated as a parallel composition of five multi-layer MPPs with different layers. The absorption coefficients of the structure have been computed under plane wave conditions using the TMM and the FEM methods, and the numerical results are matched perfectly. The results show that the multi-layer MPP structure can guarantee a high absorption rate (consistently over 90%) in the frequency range of 400~5000 Hz. The sound absorption mechanism of the multi-layer MPP structure was investigated using the acoustic impedance and the reflection coefficient of the complex frequency surface. In addition, the proposed structure is a subwavelength absorber because the low-frequency wavelengths in the air are 12 times larger in magnitude than the overall length of the structure and 31 times larger in volume than the width of the prototype.

Conflict of interest statement

The authors reported no potential conflict of interest.

Acknowledgments

This study was supported by the National Science Foundation of China (NSFC) under the grant no. 12104386; The science and technology innovation Program of Hunan Province under the grant no. 2021RC2097; The Guangdong Basic and Applied Basic Research Fund Regional Joint Fund Youth Fund Project under the grant no. 2019A1515111118; China Postdoctoral Science Foundation under the grant no. 2022M711354; Natural Science Foundation of Hunan Province Youth Project under the grant no. 2022JJ40421.

References

1. Bucciarelli F., Malfense Fierro G.P., Meo M. (2019), A multilayer microperforated panel prototype for broadband sound absorption at low frequencies, *Applied Acoustics*, **146**: 134–144, doi: 10.1016/j.apacoust.2018.11.014.
2. Carbajo J., Ghaffari Mosanenzadeh S., Kim S., Fang N.X. (2020), Multi-layer perforated panel absorbers with oblique perforations, *Applied Acoustics*, **169**: 107496, doi: 10.1016/j.apacoust.2020.107496.
3. Cheng B., Gao N., Huang Y., Hou H. (2022), Broadening perfect sound absorption by composite absorber filled with porous material at low frequency, *Journal of Vibration and Control*, **28**(3–4): 410–424, doi: 10.1177/1077546320980214.
4. Cheng Y. (2018), Acoustic absorption of a microperforated panel without the backing cavity, [in:] *INTER-NOISE and NOISE-CON Congress and Conference Proceedings*, pp. 171–180.
5. Cobo P., de la Colina C., Roibás-Millán E., Chimeno M., Simón F. (2019), A wideband triple-layer microperforated panel sound absorber, *Composite Structures*, **226**: 111226, doi: 10.1016/j.compstruct.2019.111226.
6. Cui H., Hu Z., Hu H. (2022), Research on the low-frequency sound absorption characteristics of coiled Helmholtz cavity acoustic metamaterials, *Advances in Mechanical Engineering*, **14**(8), doi: 10.1177/16878132221119996.
7. Gao N., Wu J.H., Hou H., Yu L. (2017), Excellent low-frequency sound absorption of radial membrane acoustic metamaterial, *International Journal of Modern Physics B*, **31**(03): 1750011, doi: 10.1142/S0217979217500114.
8. Jiménez N., Romero-García V., Pagneux V., Groby J.-P. (2017a), Quasiperfect absorption by subwavelength acoustic panels in transmission using accumulation of resonances due to slow sound, *Physical Review B*, **95**(1): 014205, doi: 10.1103/PhysRevB.95.014205.
9. Jiménez N., Romero-García V., Pagneux V., Groby J.-P. (2017b), Rainbow-trapping absorbers: Broadband, perfect and asymmetric sound absorption by subwavelength panels for transmission problems, *Scientific Reports*, **7**(1): 13595, doi: 10.1038/s41598-017-13706-4.
10. Lee D.H., Kwon Y.P. (2004), Estimation of the absorption performance of multiple layer perforated panel systems by transfer matrix method, *Journal of Sound*

and Vibration, **278**(4–5): 847–860, doi: 10.1016/j.jsv.2003.10.017.

11. Li C. (2018), Sound absorption of microperforated panels in complex vibroacoustic environments, [in:] *INTER-NOISE and NOISE-CON Congress and Conference Proceedings*, pp. 6237–6249.
12. Li Y., Assouar B.M. (2016), Acoustic metasurface-based perfect absorber with deep subwavelength thickness, *Applied Physics Letters*, **108**(6): 063502, doi: 10.1063/1.4941338.
13. Liu C.R., Wu J.H., Chen X., Ma F. (2019), A thin low-frequency broadband metasurface with multi-order sound absorption, *Journal of Physics D: Applied Physics*, **52**(10): 105302, doi: 10.1088/1361-6463/aafaa3.
14. Liu C.R., Wu J.H., Yang Z., Ma F. (2020), Ultra-broadband acoustic absorption of a thin microperforated panel metamaterial with multi-order resonance, *Composite Structures*, **246**: 112366, doi: 10.1016/j.compstruct.2020.112366.
15. Maa D.-Y. (1983), Direct and accurate impedance measurement of microperforated panel, [in:] *INTER-NOISE and NOISE-CON Congress and Conference Proceedings*, pp. 363–366.
16. Maa D.-Y. (1984), Wide-band sound absorber based on microperforated panels, [in:] *INTER-NOISE and NOISE-CON Congress and Conference Proceedings*, pp. 415–420.
17. Maa D.-Y. (1994), Microperforated panel at high sound intensity, [in:] *INTER-NOISE and NOISE-CON Congress and Conference Proceedings*, pp. 1511–1514.
18. Maa D.-Y., Liu K. (2000), Sound absorption characteristics of microperforated absorbers for random incidence, *Chinese Journal of Acoustics*, **19**(4): 289–298, doi: 10.15949/j.cnki.0217-9776.2000.04.001.
19. Maa D-Y. (1998), Potential of microperforated panel absorber, *The Journal of the Acoustical Society of America*, **104**(5): 2861–2866, doi: 10.1121/1.423870.
20. Mosa A.I., Putra A., Ramlan R., Esraa A.-A. (2020a), Absorption coefficient of a double-layer inhomogeneous micro-perforated panel backed with multiple cavity depths, *Acoustics Australia*, **48**(1): 69–78, doi: 10.1007/s40857-020-00176-4.
21. Mosa A.I., Putra A., Ramlan R., Esraa A.-A. (2020b), Wideband sound absorption of a double-layer microperforated panel with inhomogeneous perforation, *Applied Acoustics*, **161**: 107167, doi: 10.1016/j.apacoust.2019.107167.
22. Prasetiyo I., Sihar I., Sudarsono A.S. (2021), Realization of a thin and broadband microperforated panel (MPP) sound absorber, *Applied Acoustics*, **183**: 108295, doi: 10.1016/j.apacoust.2021.108295.
23. Rafique F., Wu J.H., Liu C.R., Ma F. (2022), Low-frequency sound absorption of an inhomogeneous micro-perforated panel with j-shaped cavities of different depths, *Acoustics Australia*, **50**(2): 203–214, doi: 10.1007/s40857-021-00261-2.
24. Rafique F., Wu J.H., Waquas M., Lushuai X., Ma F. (2021), A thin double-layer multiple parallel-arranged inhomogeneous microperforated panel absorber for wideband low-frequency sound absorption, *Journal of the Brazilian Society of Mechanical Sciences and Engineering*, **44**(1): 1–18, doi: 10.1007/S40430-021-03327-4.
25. Romero-García V., Theocharis G., Richoux O., Pagneux V. (2016), Use of complex frequency plane to design broadband and sub-wavelength absorbers, *The Journal of the Acoustical Society of America*, **139**(6): 3394–3402, doi: 10.1121/1.4950708.
26. Shao H., He J., Zhu J., Chen G., He H. (2022), Low-frequency sound absorption of a tunable multilayer composite structure, *Journal of Vibration and Control*, **28**(17–18): 2279–2287, doi: 10.1177/10775463211008279.
27. Wu F., Xiao Y., Yu D., Zhao H., Wang Y., Wen J. (2019), Low-frequency sound absorption of hybrid absorber based on micro-perforated panel and coiled-up channels, *Applied Physics Letters*, **114**(15): 151901, doi: 10.1063/1.5090355.
28. Xiaoqi Z., Cheng L. (2021), Broadband and low frequency sound absorption by Sonic black holes with micro-perforated boundaries, *Journal of Sound and Vibration*, **512**: 116401, doi: 10.1016/j.jsv.2021.116401.
29. Xie S., Yang S., Yan H., Li Z. (2022), Sound absorption performance of a conch-imitating cavity structure, *Science Progress*, **105**(1): 00368504221075167, doi: 10.1177/00368504221075167.
30. Zhao L., Lin T.R. (2022), A turned double-layer microperforated panel for low frequency sound absorption in enclosures with limited cavity space, *Applied Acoustics*, **188**: 108594, doi: 10.1016/j.apacoust.2021.108594.